



Electrical Facility Effects on Hall Current Thrusters: Electron Termination Pathway Manipulation

Jonathan A. Walker,* Samuel J. Langendorf,[†] and Mitchell L. R. Walker[‡]
Georgia Institute of Technology, Atlanta, Georgia 30332

Vadim Khayms[§]
Lockheed Martin Space Systems Company, Sunnyvale, California 94089
and

David King[¶] and Peter Pertson**
Aerojet Rocketdyne, Inc., Redmond, Washington 98052

DOI: 10.2514/1.B35904

A nonnegligible fraction of the charged particles in the Hall current thruster plume completes the electrical circuit through the conductive wall of a ground-based vacuum test facility. The resultant electrical circuit is different from the electrical circuit completed by the Hall current thruster in the onorbit environment. To understand the electrical circuit created in ground-based testing, this work examines the effect of an electrically biased metal plate, placed in the far-field plume of a Hall current thruster, on the plasma plume characteristics, the Hall current thruster thrust, and the electron termination pathways. An Aerojet Rocketdyne T-140 Hall current thruster is operated at 300 V and 10.3 A on xenon propellant. The operational neutral background pressure is 7.3×10^{-6} torr, corrected for xenon. Two aluminum plates, one representative of the radial wall of the vacuum chamber and one representative of the axial wall of the vacuum chamber, are placed 2.3 m radially outward from the thruster centerline and 4.3 m axially downstream from the discharge channel exit plane, respectively. At each axial bias plate voltage, measurements of thrust, electrical characteristics of the Hall current thruster, thruster body electrical waveform, and radial-axial plate waveforms are recorded. A Langmuir probe, a Faraday probe, and an emissive probe are placed 1 m downstream of the Hall current thruster exit plane. The cathode-to-ground voltage and plasma potential behavior closely follow the trends observed from in-flight measurements of the Small Missions for Advanced Research in Technology-1 PPS-1350 Hall current thruster. This investigation experimentally quantifies the impact of the varying in-flight plasma plume conditions on Hall current thruster operation in a ground-based vacuum facility.

I. Introduction

ELECTRIC propulsion (EP) flight qualification and lifetime testing typically occur in electrically conductive ground-based vacuum chamber test facilities. Electrically conductive test facilities present a unique challenge to EP devices because the electrically grounded wall boundary imposed by the vacuum facilities is not representative of the flight environment. Traditionally, operational background neutral pressure corrections are used as a means to translate ground-based Hall current thruster (HCT) behavior to expected flight operation [1–11]. Recent work on the HCT suggests that pressure considerations may not entirely capture the effect of the vacuum chamber environment on HCT operation [12–17].

Flight data from the Russian Express satellites' north–south and east–west station-keeping SPT-100 HCTs revealed an expanded in-space plume that was not measured in ground testing [15]. The expanded plume of the SPT-100 had high-energy ions in the offaxis plume of the HCT and created anomalous disturbance torques due to impingement of these high-energy ions on satellite surfaces [15]. This behavior has been attributed, but not yet demonstrated, to be the result of facility enhanced charge–exchange collisions removing energetic offaxis ions from the population [15,18]. These high-energy ions were not measured in ground testing due to the increased presence of charge–exchange ions in the vacuum facility environment. Anomalous thruster behavior was also experienced during the European Space Agency's Small Missions for Advanced Research in Technology-1 (SMART-1) mission using the PPS-1350 HCT. The PPS-1350 HCT showed periods of positive cathode-to-satellite-bus common voltage during times of elevated in-space plasma potential measurements [12,13,19]. The causes of these elevated in-space plasma potential measurements were attributed to exposure of low-voltage solar panel contacts to the HCT plume [12]. To the best of the authors' knowledge, this behavior has not been replicated in a ground-based testing environment.

Previous work by Frieman et al. showed that HCT cathode-to-ground voltage was susceptible to the influence of a downstream bias plate [20] and concluded that the conductive vacuum chamber was indeed part of the HCT electrical circuit through the mediation of the electron-ion loss rate of the plume. However, plume and performance measurements were not taken. Further investigation by Frieman et al. [17] identified three electron termination circuits: downstream axial surfaces, downstream radial surfaces, and the thruster body. By increasing the cathode radial position away from HCT centerline, the magnitude of the electron current collected on the radial chamber plate surfaces increased, indicating increased electron termination on the radial walls of the vacuum facility. Figure 1 shows a graphical representation of the electron termination pathways. It is important to note that the resistors shown in Fig. 1 are done to help illustrate the electron termination pathways in the facility testing, and the plasma

Received 2 June 2015; revision received 29 February 2016; accepted for publication 8 June 2016; published online 31 August 2016. Copyright © 2016 by Jonathan A. Walker, Samuel J. Langendorf, and Mitchell L. R. Walker. Published by the American Institute of Aeronautics and Astronautics, Inc., with permission. Copies of this paper may be made for personal and internal use, on condition that the copier pay the per-copy fee to the Copyright Clearance Center (CCC). All requests for copying and permission to reprint should be submitted to CCC at www.copyright.com; employ the ISSN 0748-4658 (print) or 1533-3876 (online) to initiate your request.

*Graduate Research Assistant, Aerospace Engineering, High-Power Electric Propulsion Laboratory; jwalker30@gatech.edu. Student Member AIAA.

[†]Graduate Research Assistant, Aerospace Engineering, High-Power Electric Propulsion Laboratory; samuel.langendorf@gatech.edu. Student Member AIAA.

[‡]Associate Professor, Aerospace Engineering, High-Power Electric Propulsion Laboratory; mitchell.walker@ae.gatech.edu. Associate Fellow AIAA.

[§]Electric Propulsion Architect; vadim.khayms@lmco.com. Member AIAA.

[¶]Technical Fellow, Engineering; david.king@rocket.com. Member AIAA.

**Project Engineering Specialist, Engineering; peter.peterson@rocket.com. Senior Member AIAA.

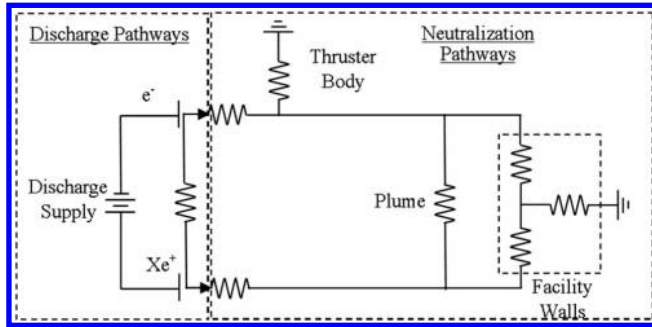


Fig. 1 Notional diagram of discharge circuit of Hall current thruster and electron termination pathways in a ground-testing environment.

of the HCT makes these pathways much more dynamic than a simple resistive path. Plume measurements show an increase in plasma potential with increased electron termination on radial walls. Their findings indicated that electron magnetization near the cathode orifice played a significant role in what the available electron termination pathways are, but they were not able to measure a time-averaged influence of the electron termination pathways on the thrust of the HCT.

From the prior work, the exact impact of the artificial boundary condition imposed by the facility walls on the HCT electrical circuit is unclear. In the flight environment, the HCT plume does not typically encounter these artificial termination sites [18]. Work done by Frieman et al. showed that the HCT floating circuit voltage relative to ground changed synchronously with changes in the downstream potential of the axial chamber plate [20]. The work did not measure plume characteristics or thrust. However, they concluded that the plasma potential changed with the bias voltage of the downstream plate, and the thrust generated by the HCT would not be affected. The changing plasma potential would also affect electron current collection at the radial walls of the vacuum chamber. The changing plasma potential might have an impact on the discharge current oscillations of the HCT, as work from Walker et al. [21] showed that the discharge current oscillation frequency and full-width/half-maximum of the discharge current oscillation frequency changed along with changes in the electron flux to the radial chamber plate.

Time-resolved measurements of the discharge current by Walker et al. [21] revealed that the discharge current oscillation frequency and full-width/half-maximum depended on cathode position. Their results also indicated that the electron Hall parameter near the cathode orifice played an important role in determining the frequency, peak to peak, and full-width/half maximum of the discharge current oscillations. These changes in the discharge current were also measured on the time-resolved current waveforms of the chamber witness plates, and they demonstrated a strong statistical correlation between the HCT discharge current and the chamber plates that were independent of the magnitude of the electron Hall parameter at the cathode orifice.

With previous cathode positioning work done by Frieman et al. [17] and Walker et al. [21], it is difficult to separate the effect of the cathode position and the electron termination pathways on the HCT. The methodology of Frieman et al. [20] by electrically biasing the downstream chamber plate presented a possible way to precisely control the influence of the electron termination pathways on the HCT electrical circuit. The biased downstream chamber plate had already shown that it could influence the floating voltage of the HCT, which was similar to the behavior seen during the SMART-1 mission. The lack of precise knowledge of plume plasma potential prevented direct comparison between the prior work of Frieman et al. [20] and the results obtained from the SMART-1 mission [13]. To better understand the influence of the electron termination pathways on the HCT electrical circuit and its connection to the in-flight environment, it is the goal of this investigation to better understand the impact of electrically biasing the downstream axial plate on the HCT performance, plume characteristics, and electron termination pathways.

II. Experimental Apparatus

A. Vacuum Facility

All experiments were performed in Vacuum Test Facility 2 (VTF-2) at the Georgia Institute of Technology's High-Power Electric Propulsion Laboratory. Figure 2 shows a schematic of this facility. VTF-2 is a stainless-steel chamber measuring 9.2 m in length and 4.9 m in diameter. VTF-2 was evacuated to a rough vacuum using one 495 cubic feet per minute (CFM) rotary-vane pump and one 3800 CFM blower. High vacuum was achieved using 10 liquid-nitrogen-cooled CVI TM1200i reentrant cryopumps. The cryopump shrouds were fed using the Stirling Cryogenics SPC-8 RL special closed-loop nitrogen liquefaction system, detailed by Kieckhafer and Walker [22]. The facility had a combined nominal pumping speed 350,000 l/s on xenon and could achieve a base pressure of 1.9×10^{-9} torr. Pressure in VTF-2 was monitored using two Agilent Bayard Alpert (BA) 571 hot filament ionization gauges controlled by an Agilent XGS-600 gauge controller. The pressure measurement uncertainty of the Agilent BA 571 was expected to be $\pm 20\%$, which was -10% of the indicated pressure [23]. One gauge was mounted to a flange on the exterior of the chamber, whereas the other was mounted 0.6 m radially outward from the thruster centered on the exit plane. To prevent plume ions from having a direct line of sight to the ionization gauge filament of the interior ion gauge, and potentially affect the pressure measurement, a gridded neutralizer assembly identical to the one used by Walker and Gallimore [1] was attached to the gauge orifice. The nominal operating pressure for this work as measured by the interior and exterior ion gauges was 1.3×10^{-5} torr and 7.3×10^{-6} torr, corrected for xenon, respectively. As specified by the manufacturer, the corrected pressure P_c was found by relating the indicated pressure P_i and the vacuum chamber base pressure P_b to a gas-specific constant using the following equation [24]:

$$P_c = \frac{P_i - P_b}{2.87} + P_b \quad (1)$$

B. T-140 Hall Current Thruster

All experiments detailed in this work were performed using the Aerojet Rocketdyne T-140 HCT originally developed by Space Power, Inc., in collaboration with the Keldysh Research Center and Matra Marconi Space [25]. The T-140 HCT is a laboratory-model HCT that has a discharge channel made of M26-grade boron nitride with an outer channel diameter of 143 mm. The performance of the T-140 has been extensively mapped by prior investigations [25]. The thruster body was isolated from the facility ground such that the thruster body could be electrically configured as either floating or grounded. The resistance to ground when the thruster body was electrically grounded was measured to be less than 0.2Ω .

High-purity (99.9995%) xenon propellant was supplied to the thruster and cathode using stainless-steel lines metered with MKS Instruments 1179A mass flow controllers. The controllers were

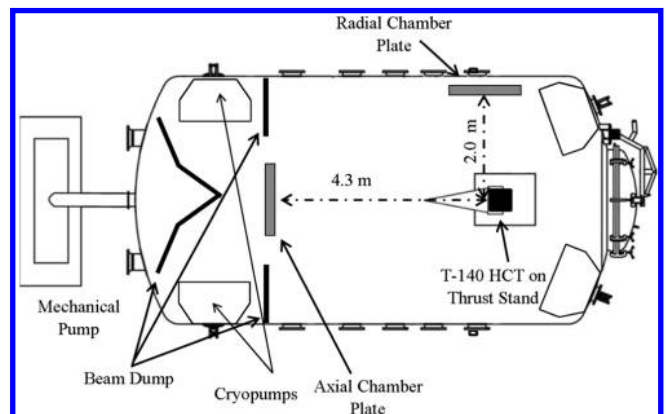


Fig. 2 Overhead view of the vacuum chamber test facility, HCT, and chamber plates.

calibrated before each test by measuring gas pressure and temperature as a function of time in a known control volume. After calibration, the mass flow controllers had an uncertainty of ± 0.03 mg/s (5.1% referenced at the tested flow rate) for the cathode flow and ± 0.12 mg/s (2% reference at the tested flow rate) for the anode flow [26].

An Electric Propulsion Laboratory hollow cathode plasma electron emitter 500-series cathode was located at the nine o'clock position of the HCT. The cathode flow rate was set to a constant 1.16 mg/s for all HCT operating conditions. The orifice location of the cathode was located approximately 2.5 cm downstream of the thruster exit plane at a fixed declination of 55 deg with respect to the thruster centerline. The nominal radial position of the cathode was 18.1 cm outward from HCT centerline. Time-resolved measurements of the discharge current, radial chamber plate current and voltage, and axial chamber plate current and voltage were taken at each axial bias plate voltage.

The T-140 HCT discharge was controlled using a Magna-Power TSA800-54 power supply. The thruster inner and outer magnet coils were powered with TDK-Lambda GEN60-25 power supplies. A TDK-Lambda Genesys 150 V/10 A and a TDK-Lambda Genesys 40 V/38 A power supply were used to power the cathode keeper and heater, respectively. The thruster discharge supply was connected to a discharge filter consisting of a 95 μ F capacitor and 1.3 Ω resistor in order to prevent oscillations over 1.4 kHz in the discharge current from reaching the discharge supply. Diagnostic and power connections entered VTF-2 through separate feedthroughs to eliminate potential crosstalk between the thruster discharge power lines and diagnostic lines. Figure 3 shows the circuit used to operate the T-140 HCT and current and voltage measurement points in this work.

The discharge current oscillations, measured on the thruster side of the discharge filter, of the T-140 HCT were recorded using a Teledyne LeCroy CP150 current probe connected to a Teledyne LeCroy HDO6104 oscilloscope. The uncertainty and bandwidth of the current probe were $\pm 1\%$ and 10 MHz; for the oscilloscope, they were $\pm 0.5\%$ full scale and 1 GHz. In the floating thruster body configuration, the thruster body floating voltage was measured differentially using Teledyne LeCroy PP018 passive probes with a bandwidth of 500 MHz and an accuracy of $\pm 0.5\%$ connected to the Teledyne LeCroy oscilloscope. When the thruster body was grounded, the current conducted through the thruster body to ground was measured using a Teledyne LeCroy CP030 current probe connected to the Teledyne LeCroy oscilloscope. The CP030 had a bandwidth of 50 MHz and an accuracy of $\pm 1\%$. A filter sensitivity analysis of the discharge current filter operating in tandem with the

discharge supply and hall thruster, as described by Spektor et al. [27], was not performed.

The mean discharge voltage of the T-140 HCT was measured differentially using a pair of Teledyne LeCroy PPE2KV 100:1 high-voltage probes connected to a Teledyne LeCroy HDO6104 Oscilloscope. The bandwidth of the voltage probes was 400 MHz; the oscilloscope had an uncertainty and bandwidth of $\pm 2\%$ and 300 MHz, respectively. This was done to ensure that the HCT electrical circuit remained floating relative to the ground. Figure 3 shows the location of each telemetry measurement in the T-140 HCT circuit.

C. Thrust Stand

Thrust was measured using the null-type inverted pendulum thrust stand of the NASA John H. Glenn Research Center design, detailed in the work of Xu and Walker [28]. The thrust stand consisted of a pair of parallel plates connected by a series of four flexures that supported the top plate and permitted it to deflect in response to an applied force. The position of the upper plate was measured using a linear voltage differential transformer (LVDT) and was controlled using two electromagnetic actuators. During operation, the current through each actuator was controlled using a pair of proportional-integral-derivative control loops that used the LVDT signal as the input and then modulated the current through the actuators in order to remove any vibrational noise (damper coil) and hold the upper plate stationary (null coil). The thrust was correlated to the resulting current through the null coil that was required to keep the upper plate stationary. To maintain thermal equilibrium during thruster firings, the thrust stand was actively cooled using three parallel loops: one each through the structure, the null coil, and the outer radiation shroud. Cooling water was supplied by a 1100 W VWR International 1173-P refrigerated recirculation chiller and did not vary by more than 5°C as compared to the thruster-off condition [28]. The thrust stand was calibrated by loading and offloading a set of known weights that spanned the full range of expected thrust values. A linear fit was then created in order to correlate the null coil current to the force applied to the thrust stand. To minimize the thermal drift of the zero position, the T-140 HCT was initially fired for 3 h at the 3.1 kW nominal operating point to permit initial heating of the system to near-thermal equilibrium [25] before the first calibration and was then shut down every 40–60 min so that a recalibration could be performed. The thrust stand uncertainty for this work was ± 3 mN ($\pm 1.7\%$ full scale). All data were collected with the T-140 HCT operating at a discharge voltage of 300 V, a discharge power of 3.16 kW, an anode xenon flow rate of 11.6 mg/s, and a cathode xenon flow rate of 1.16 mg/s. The thruster discharge voltage, inner and outer magnet currents, anode mass flow rate, and cathode mass flow rate were held constant for all test configurations.

D. Configuration of Plates

To assess the impact of the conductive walls of the vacuum chamber facility on HCT operation, two 0.91 m \times 0.91 m \times 0.16-cm-thick square aluminum plates served as representative chamber surfaces. Each plate was mounted adjacent to, but electrically isolated from, the walls of the vacuum test facility. One plate was placed 4.3 m downstream from the exit plane of the thruster, and it is referred to as the "axial chamber plate" or "axial plate." The other plate was located 2.3 m radially outward from the thruster centerline and centered on the exit plane of the T-140 HCT, and it is referred to as the "radial chamber plate" or "radial plate." These two locations were chosen because each location was representative of unique plasma environments: inside the HCT beam and outside the HCT beam 95% half-angle [29]. The axial plate was in a quasi-neutral plasma environment composed primarily of accelerated HCT ions and electrons, and the radial plate was in a quasi-neutral plasma environment primarily composed of charge-exchange ions and electrons. Figure 2 shows the physical location of the plates with respect to the T-140 HCT. Identical plates have been used in previous studies of electrical facility effects [17,20,21]. The radial chamber plate was electrically grounded using RG-58 coaxial cable with a grounded shield that passed through a Bayonet Neill-Concelman feedthrough into the chamber. The resistance between the

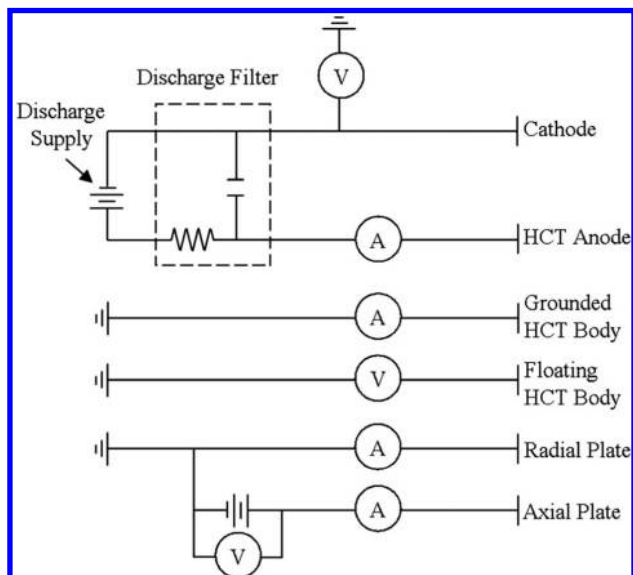


Fig. 3 Electrical diagram of current and voltage measurements of the HCT discharge circuit.

radial chamber plate and the chamber walls was measured to be 1.1Ω . Based on current measurements made by Frieman et al. [17,20], the current capacity of the inner conductor of the RG-58 was sufficient for radial plate current collection and would not pose any thermal issues during thruster testing. For radial plate current measurements, ground loops were not a concern because the current probes were active clamp current monitors. The axial chamber plate was biased relative to the ground using a TDK Gen 60 V and 12.5 A power supply. To avoid thermal issues with maintaining the axial plate bias voltage, the axial chamber plate was connected to the power supply via 6-AWG copper wire that connected to a 150 A power vacuum feedthrough. During this investigation, the axial plate current did not exceed 10 A for testing conditions. The resistance between the axial chamber plate and the chamber walls was measured to be less than 0.2Ω .

The current and voltage waveforms of the axial chamber plate were measured using a LeCroy CP030 current clamp and a PP005A 10:1 voltage divider connected to a Teledyne LeCroy HDO6104 oscilloscope. The radial chamber plate was connected to the chamber ground with the current conducted to the ground measured with a Teledyne LeCroy CP030 current sensor connected to a Teledyne LeCroy HDO6104 oscilloscope; the plate currents and thruster telemetry waveforms were measured simultaneously at a sampling frequency of 125 MS/s (Mega-samples per second) for a 20 ms window to ensure that multiple fundamental discharge current mode periods were captured.

E. Plume Diagnostics

Plume diagnostics were taken along a $1\text{ m} \pm 0.01\text{ m}$ radius centered at the thruster centerline and discharge plane. Ion current density measurements occurred throughout a full range of 180 deg, whereas emissive probes and Langmuir probes sweeps were taken at select angular positions based on the ion current density profile of the HCT plume. A schematic overview of the plume diagnostics relative to the

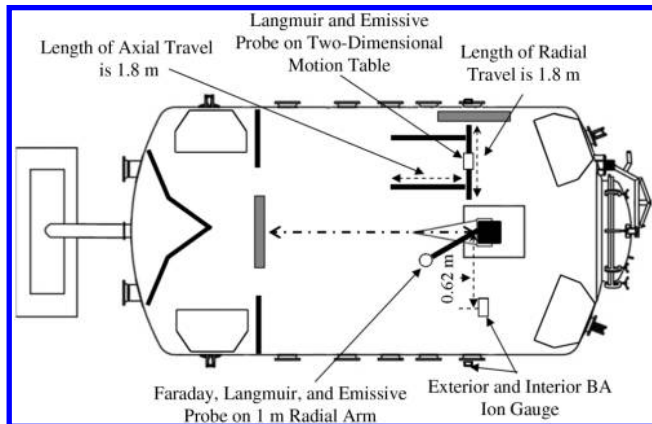


Fig. 4 Overhead view of the vacuum chamber test facility, HCT, and plume diagnostics.

HCT is shown in Fig. 4. The probe diagnostics were mounted to a Parker Daedel RT-series 8 in. rotary motion table. All three of the plume diagnostics (a Langmuir probe, a Jet Propulsion Laboratory (JPL) nude-style Faraday probe, and an emissive probe) were attached in an array on a radial probe arm. The arms of the array were angled such that the probe-to-probe centerline linear distance was at $0.17 \pm 0.01\text{ m}$ apart and remained at a 1 m radial distance throughout the probe arm sweep. Figure 4 shows the relative position of the diagnostics arm, and Figs. 5 and 6 show a photograph and notional diagram, respectively, of the probe arrangement on the diagnostics arm.

1. Emissive Probe

The probe tip used for this work was constructed from a loop of 0.13 mm thoriated-tungsten wire housed in a 4.8 mm double-bore alumina tube. Emissive probe sweeps were performed at select thruster-to-centerline angles at a radius of 1 m from the thruster centerline and discharge exit plane. The inflection point method was used for data collection. In this method, the probe was heated and then the emission current was monitored as the probe bias voltage was swept in a manner similar to that used with Langmuir probes. The changing characteristic of the emission current trace as a function of applied bias voltage was then used to determine the plasma potential [30]. During each measurement, the heating current to the emissive probe filament was held at five different heating current values to change the electron emission of the probes. These heating current values varied throughout the probe lifetime but were within a range between 1.2 and 1.8 A. One bias voltage sweep was taken per emissive probe filament heating current. During each bias voltage sweep, the probe voltage was varied over a range of 0 to 100 V in 1 V increments, with a 300 ms dwell time. The inflection point was then found in each of the Current-Voltage (I-V) traces for each of the different heating current levels, and the plasma potential was found by linearly extrapolating these values to zero emission [30]. The uncertainty associated with this method was approximately $\pm 0.5\text{ V}$ [30]. The heating current was controlled using a Xantrex XPD 60-9 power supply. The probe bias was controlled by a Keithley 2410 1100 V source meter, and the emission current was measured using a Keithley 6487 picoammeter. The source meter and picoammeter were simultaneously controlled using a LabView virtual instrument to ensure synchronous recording of the probe bias voltage and emitted current.

2. Langmuir Probe

The ion and electron number densities were measured using a cylindrical Langmuir probe. Langmuir probe sweeps were performed at select thruster-to-centerline angles at a radius of 1 m from the thruster centerline and discharge exit plane. The probe used in this work was constructed using a 0.13-mm-diam, 18.3-mm-long tungsten tip housed inside an alumina tube. The probe was bent at a right angle, such the probe tip was not pointed at the HCT and was pointed 90 deg out of the plane of the probe arm sweep. The bend in the probe was done to minimize the effect of the probe tip on the I-V trace of the

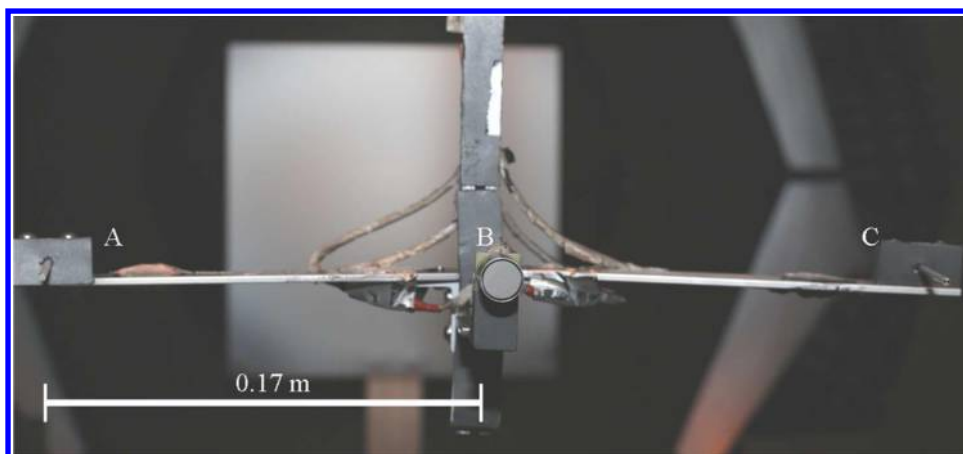


Fig. 5 Probe arm with plume diagnostics attached Langmuir probe (A), Faraday probe (B), and emissive probe (C).

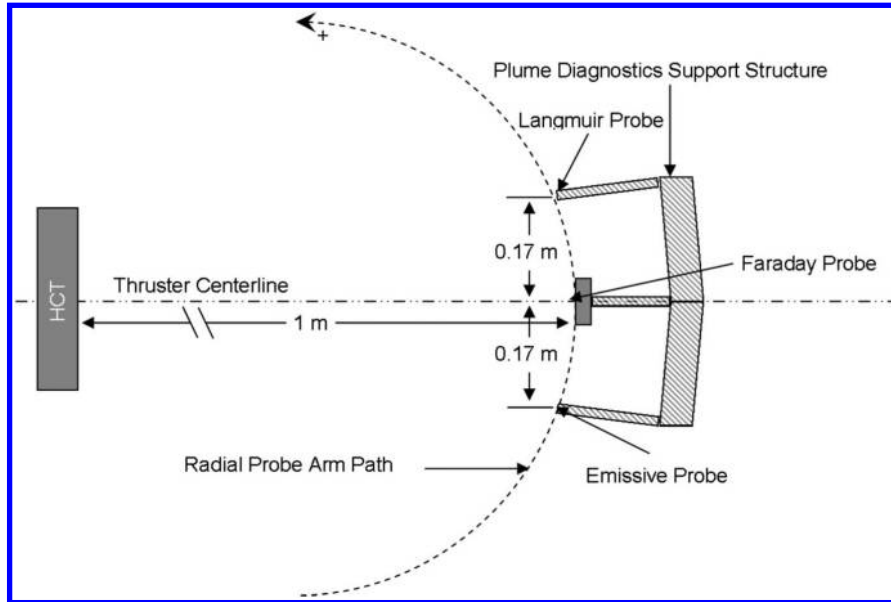


Fig. 6 Overhead view of notional layout of the radial diagnostics probe arm.

Langmuir probe. A Keithley 2410 1100 V source meter was used to control the probe tip bias and measure the collected current. During each current-voltage sweep, the tip voltage was varied over a range of -50 to 100 V in 0.2 V increments, with a 300 ms dwell time. For low axial plate bias voltage, ion saturation occurred near 12 V; and at higher axial plate bias voltage, ion saturation occurred near the potential of the downstream axial chamber plate. Two sweeps were taken per measurement and were averaged together before processing. The results were interpreted using an orbital-motion-limited theory, with an expected uncertainty in ion and electron density measurements of $\pm 40\%$ [31,32].

3. Faraday Probe

The ion current density was measured using a nude-type JPL Faraday probe [33]. Faraday probe measurements occurred continuously along a 180 deg, 1 m \pm 0.01 m arc. Angular resolution during the sweep was limited by the multiplexor hardware-required settling time given a measurement voltage range. Angular resolution ranged from 0.34 deg in the “wings” of the plume to 0.2 deg in the center of the HCT plume. The diameter of the collector was 2.31 cm. The probe had a guard-ring diameter of 2.54 cm with a 0.036 cm gap between the collector and the guard ring. The guard ring and collector were biased to -30 V below ground for all axial plate bias voltages. To measure the current flowing to the collector, the voltage drop across a $100\Omega \pm 12\%$ precision resistor was measured using an Agilent 34980A Mainframe with an Agilent 34922 A armature multiplexor. Rotary table encoder information and voltage drop measurements were taken using a LabView virtual instrument to ensure the synchronous recording of the angular position and voltage drop across the shunt resistor. Data reduction and correction factors used to calculate the ion current density from the Faraday probe data were performed according to the work of Brown [34] and Brown and Gallimore [35].

III. Results

This section introduces the overall trends of each of the diagnostics before discussing the impact on biasing of the axial plate on the electrical facility effects. The following section covers the impact of the axial chamber plate on the HCT cathode-to-ground voltage (HCT circuit floating potential), the HCT plume, and the radial plate current collection.

A. Axial Chamber Plate Behavior

As shown in Fig. 7, the axial chamber plate current collection behavior exhibited three distinct regions. Because the plate was biased with a positive voltage relative to the ground, the current

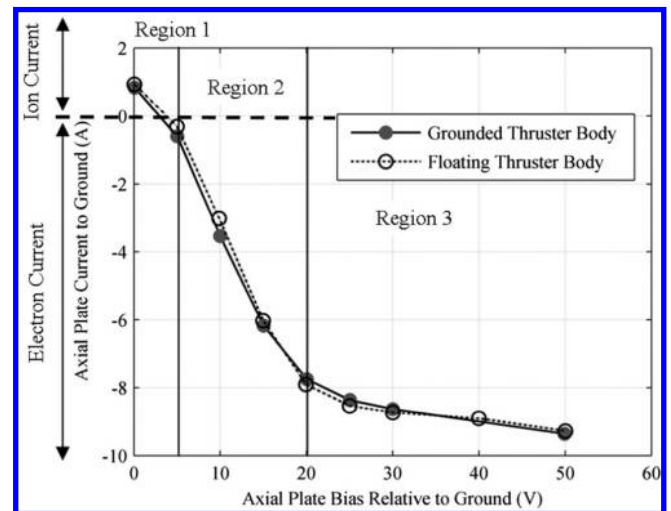


Fig. 7 Axial chamber plate current collected as a function of axial plate bias voltage. Error bars are encompassed by plot markers.

collected on bias plate transitioned from a net flux of ions to a net flux of electrons. With the axial chamber plate bias at 0 V, the beam ions generated by the HCT composed the majority of the net charge flux to the plate. As the bias voltage increased, more electrons were gathered to the axial chamber plate. Between 0 and 5 V, sufficient electrons were collected by the plate such that there was no net charge flux to the plate. This voltage was also known as the floating voltage of the axial plate and was not precisely measured during this study. Based on the measurements of Frieman et al. [17], the floating voltage of the axial plate was expected to be approximately 4 V. At the axial chamber plate bias beyond the floating voltage, there was a net electron current collection reaching the axial chamber plate. This increase in electron current continued monotonically until the net electron current collection approached the beam current of the HCT. Based on the acceleration voltage and the thrust measured by Frieman et al. [17], the beam current of the HCT can be estimated as follows [29]:

$$I_b = \frac{T_{\text{HCT}}}{\sqrt{2MV_b}} \quad (2)$$

where I_b is the beam current, T_{HCT} is the thrust produced by the HCT, M is the mass of a xenon atom, and V_b is the acceleration potential.

Using this model, the beam current is estimated to be near 7 A. This relationship neglects the presence of multiply charged ions and does not take into account the beam divergence. Based on $E \times B$ measurements by Ekholm and Hargus [36] running a BHT-200 HCT at 250 V, a lower range to the beam current estimate can be made, and it is expected that the T-140 HCT operated at 300 V will have a doubly charged xenon population that is approximately 12% of the total ion population. This reduces the estimated beam current to be on the order of 6 A. A better estimate of the beam current is not possible using the Faraday probe because testing occurs at one operating background pressure. Without current density profile measurements at multiple background pressures, it is not possible to extrapolate the vacuum current density profile, thus making the beam current measurement via an integrated current profile artificially inflated.

For an axial plate bias greater than 20 V, the slope of the electron current collection vs axial plate bias voltage decreases by approximately 85%. Data collection above the axial chamber plate bias of 50 V above ground is not possible due to arcing events on grounded surfaces within the vacuum chamber. After raising the potential of the axial chamber plate past the floating voltage of the chamber plate, the axial chamber plate begins collecting a net flux of beam electrons from the surrounding plasma. As the plasma sheath begins to expand to collect more electrons, the plasma potential begins to increase. Once the axial chamber plate begins to collect a net electron current, the electron current collection as a function of the axial bias plate voltage above ground begins to level off, forming a knee in the curve.

The floating thruster body and the grounded thruster body configurations have similar overall current collection behaviors. At thruster body biases between 0 and 15 V, however, the floating thruster body configuration has an axial chamber plate current collection 49% and 15% smaller current than comparable grounded thruster body configurations. At greater than 15 V of the axial plate bias voltage above ground, the floating thruster body configuration has an axial chamber plate current collection 1–2% greater than comparable grounded thruster body configurations. The reason for the discrepancy between the thruster body configurations is not yet clear.

B. Radial Plate Facility Interaction

As seen in prior work, the grounded radial chamber plate collects a net flux of electron current [17]. As the bias voltage of the downstream axial chamber plate increases, the electron current collected on the radial plate decreases. Figure 8 shows the radial chamber plate current collection as a function of axial chamber plate bias voltage. The negative current collected corresponds to the net

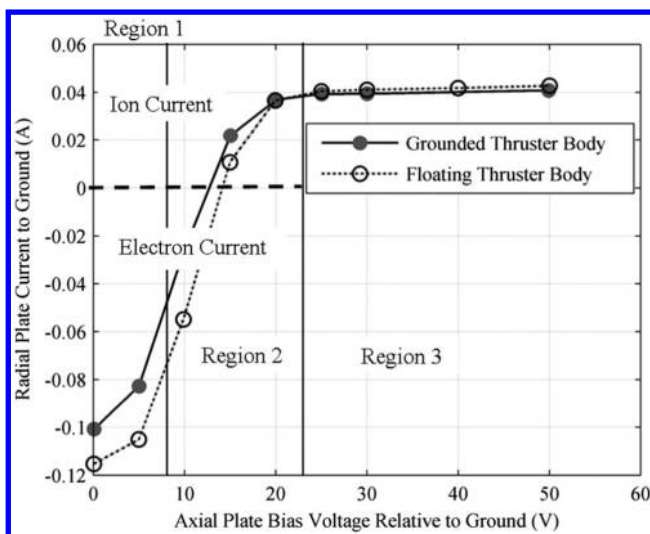


Fig. 8 Radial chamber plate current collection as a function of axial chamber plate bias voltage relative to ground. Error bars are encompassed by plot markers.

electron current, and the positive current collected indicates the net ion current.

Between 10 and 15 V of the axial chamber plate bias potential, the current collection on the radial chamber plate transitions from a net flux of electron current to a net flux of ion current. At axial bias chamber plate biases greater than 15 V, the plasma potential near the radial chamber plate rises sufficiently relative to the chamber walls that the potential difference between the plasma and the grounded radial chamber plate repels electrons. The current collection behavior of the radial chamber plate as shown in Fig. 9 indicates that, for axial bias plate voltages greater than 25 V, electrons are driven away from the radial chamber plate, and the radial chamber only collects a net ion current.

C. Influence of the Axial Chamber Plate Bias on the HCT

The effect of the downstream bias voltage of the axial chamber plate on the HCT was measured in two ways: thrust and characteristics of the HCT electrical circuit. Measurements of the thrust showed no statistically significant change in the thrust production of the HCT circuit. Based on the conclusions drawn by Frieman et al. [20], this was expected. In Fig. 10, the cathode-to-ground voltage and centerline plasma potential measurements as a function of axial plate bias voltage above ground are shown. As the axial plate bias voltage increased, the cathode-to-ground voltage began to move synchronously with the plasma potential. The cathode-to-ground voltage relative to ground changed sign between 20 and 25 V of the axial chamber plate bias. This axial plate bias voltage range corresponded to the collected electron current on the axial chamber plate above the HCT estimated beam current. From the axial chamber plate bias of 5 to 50 V, the difference between the centerline plasma potential and the cathode-to-ground voltage remained a constant $32 \text{ V} \pm 2 \text{ V}$. Because the difference between the cathode-to-ground voltage and the plasma potential remained nearly constant, there was no expected measurable change in thrust of the HCT with the axial chamber plate bias voltage. This was confirmed with direct thrust measurements. Thrust stand measurements showed that the time-averaged thrust of the HCT remained $177 \text{ mN} \pm 3 \text{ mN}$ for all axial bias plate conditions.

D. Plume Plasma Properties

Figure 11 shows the HCT plume profile. The HCT beam and exponential decline region of the current density profile show little to no dependence on the axial chamber bias plate bias. At angular positions greater than 50 deg off the thruster centerline, elevated current densities at a high (greater than 20 V) axial plate bias relative to the ground are measured. In this region, colloquially referred to as

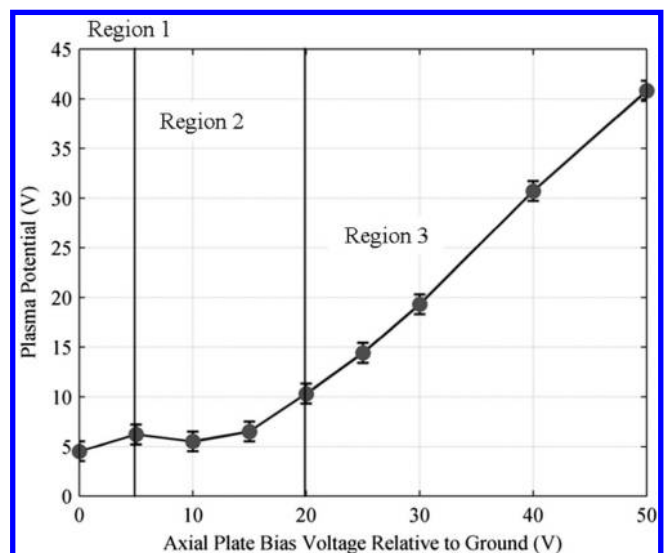


Fig. 9 Plasma potential measured at 25.4 cm radial distance away from the radial plate. Measurement is centered on radial plate centerline.

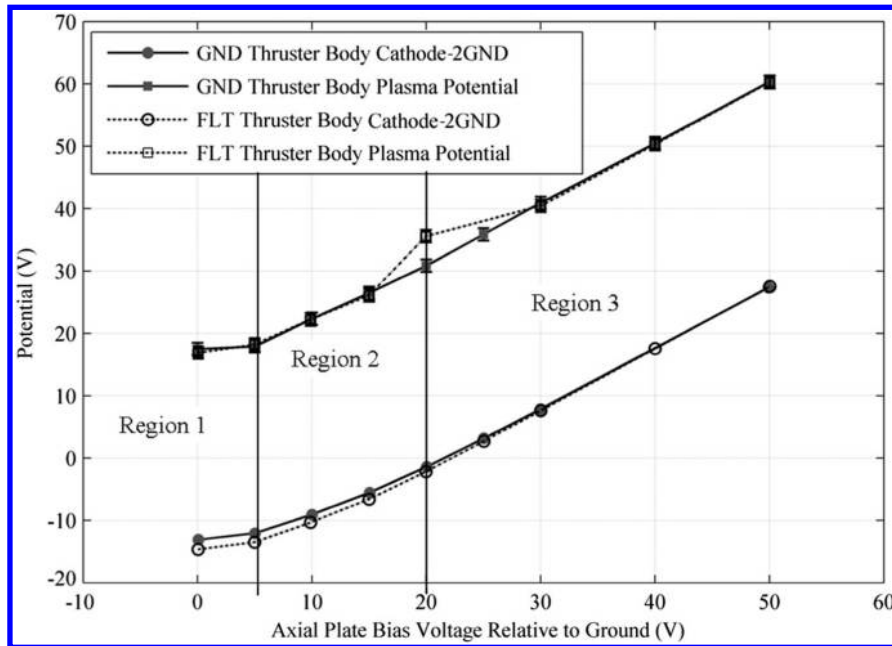


Fig. 10 Cathode-to-ground voltage and centerline plasma potential as a function of axial plate bias. Error bars for cathode-to-ground voltage are encompassed by plot markers (GND, electrically grounded; 2GND, -to ground; FLT, electrically floating).

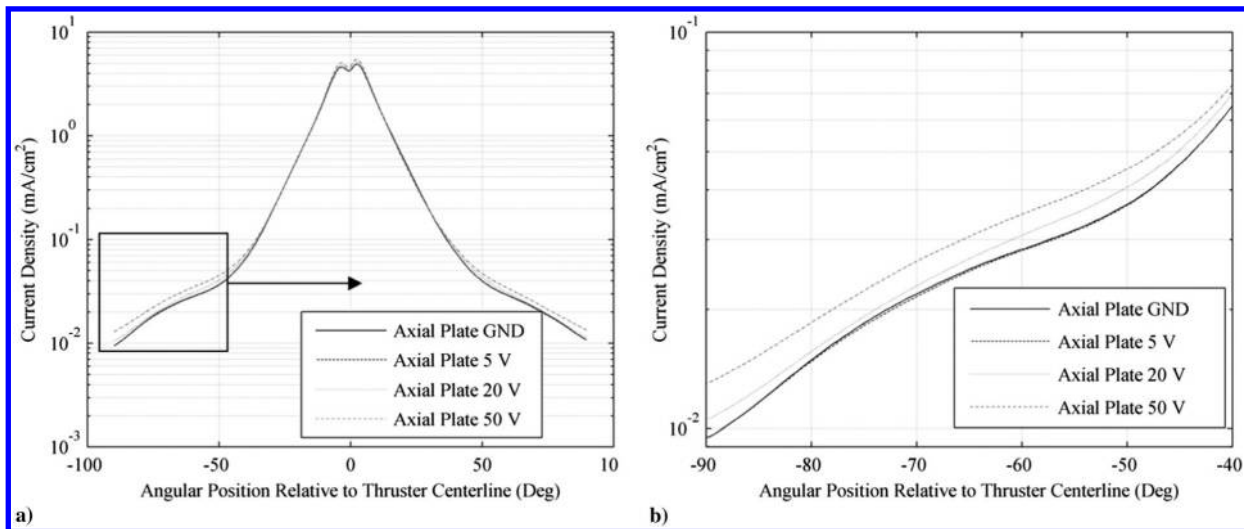


Fig. 11 Grounded thruster body HCT ion current density profile at differing axial plate bias voltages: a) full plume profile, and b) enlarged section of the plume profile.

the wings, the ions present are primarily composed of charge-exchange ions [29,34]. This region is highlighted in Fig. 11. The current density profiles of the grounded thruster body and floating thruster body show no significant differences, and so Faraday probe sweeps for the floating thruster body are not shown.

At least two Langmuir probe and emissive probe measurements were sweeps taken in each ion current density profile region: thruster centerline, exponential decline, and the wings. Assuming the plasma properties to be axisymmetric, Langmuir and emissive probe measurements were taken throughout an arc of 90 deg relative to the thruster centerline. As shown in Fig. 12, the plasma potential measurements showed a global increase in potential with respect to axial plate bias voltage. The plasma density profile showed no change outside the uncertainty of the measurement with respect to the axial plate bias voltage, as shown in Fig. 13. For both the plasma potential and ion number density, the floating thruster body configuration HCT plume profile did not show a measurable difference as compared to the grounded thruster body, and is not presented.

IV. Discussion

With the information presented in the Results section (Sec. III), it is important to begin to understand how the axial plate is able to drive global changes in the HCT testing environment. The discussion begins with examining the measured influence of the axial chamber plate bias voltage on the plasma potential and whether this impact agrees with first-order plume models. Once the impact of the axial plate bias is established, the discussion then proceeds to address the impact of the axial chamber plate on the behavior of the electron termination pathways. The discussion concludes with how the observed thruster behavior is reflective of measurements taken onorbit with the PPS-1350 HCT on the SMART-1 mission.

A. Plasma Potential and Plate Current

To better understand the interaction between the axial plate and the HCT electrical circuit, it is first important to understand the interaction between the axial plate and the thruster plume environment. Between

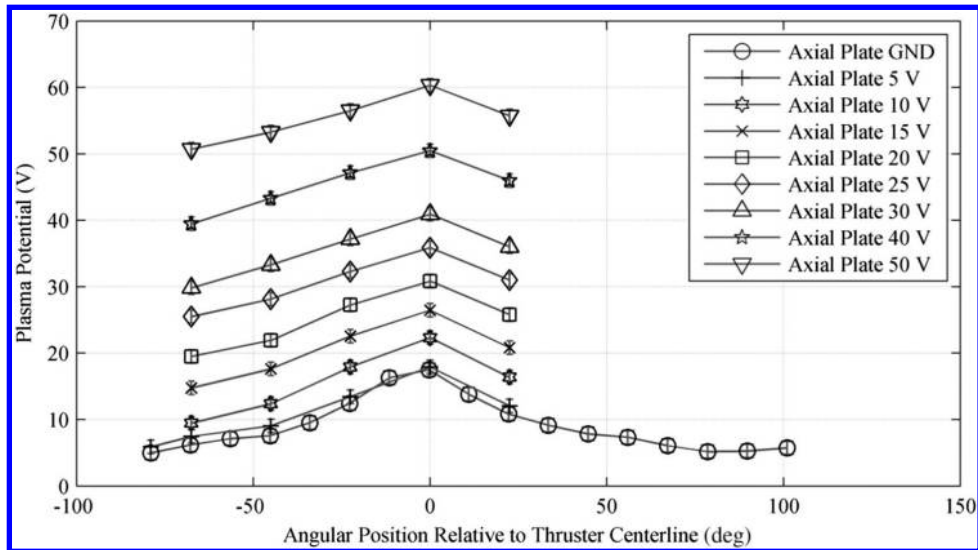


Fig. 12 Plasma potential profile as a function of axial plate bias voltage for the grounded thruster body.

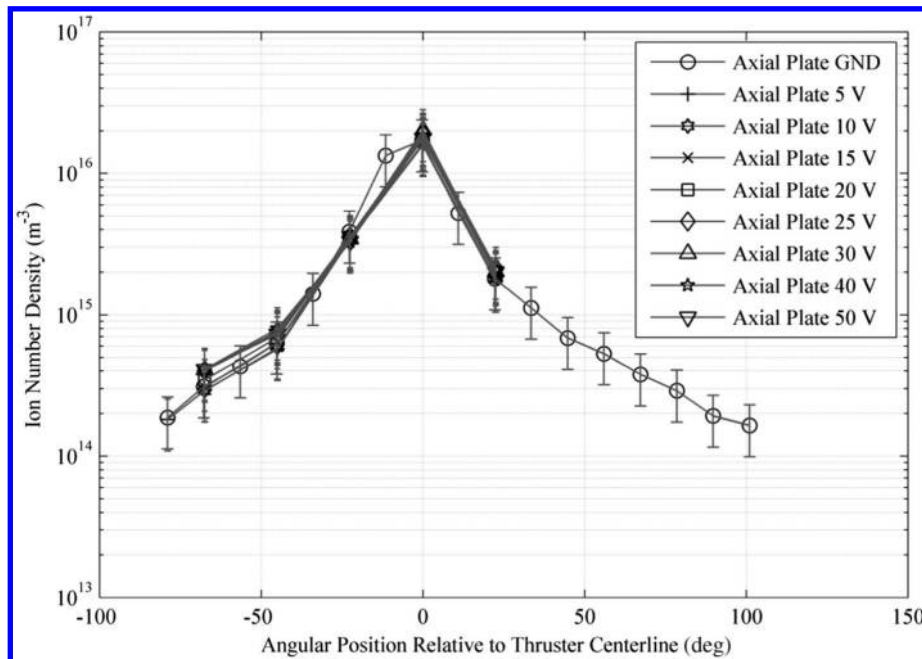


Fig. 13 Ion number density profile as a function of axial plate bias voltage.

the axial plate and the plume environment, a plasma sheath mediates the current collection. It is then critical to understand how this sheath responds to changes in the axial plate bias voltage.

Examining the data presented in Fig. 7, the current collected by the axial plate rises with bias voltage until it reaches the thruster beam current that occurs at 20 V above ground. At this potential, the plate collects an electron current equivalent to the neutralization current supplied by the cathode. Above 20 V, increases in the axial plate bias voltage result in an equal increase of the plasma potential and the floating potential of the thruster anode and cathode (Fig. 10). At these voltages, it is possible to increase the cathode potential above ground. The collected current increases slowly, as all the cathode neutralization electrons are already being collected and additional electrons must be sourced from grounded chamber surfaces. The physical connection between the two phenomena (knee in current collection and start of plasma potential rise) is the plasma charge balance. If the plate is biased positive, the plasma will electrostatically respond and the plasma potential will adjust to equalize charge loss rates and keep the plasma electrically neutral.

To illustrate the effect of the plasma charge balance and to determine if there are other sources for the additional electron current collected on the axial plate outside of the HCT beam, we model the

current collection by the plate and chamber boundary to compare to the experiment. To know the current collection, we need the local plasma parameters at the boundary. To this end, we apply the self-similar plume model of Korsun and Tverdokhlebova [37] as reported by Azziz [38]. This model neglects collisional effects in the chamber, and it assumes a two-component plasma, and adiabatic expansion of the HCT plume. The model gives the following relations to calculate the ion flux j_i , electron density n_e , electron temperature T_e , and plasma potential ϕ at any location in the plume:

$$j_{ic} = \frac{\gamma}{2\pi R^2 \tan^2 \theta_{1/2}} \frac{I_b}{v_i} \quad (3)$$

$$j_i = \frac{j_{ic}}{\cos^3 \theta (1 + (\tan^2 \theta / \tan^2 \theta_{1/2}))^{1+7/2}} \quad (4)$$

$$n_e = \frac{j_{ic}}{ev_i} \quad (5)$$

$$n_e = \frac{n_{ec}}{1 + (\tan^2 \theta / \tan^2 \theta_{1/2})} \quad (6)$$

$$\frac{T_e}{T_{ec}} = \left(\frac{n_e}{n_{ec}}\right)^{\gamma-1} \quad (7)$$

$$\phi = \phi_c - \frac{\gamma}{\gamma-1} \frac{kT_{ec}}{e} \left(1 - \left(\frac{n_e}{n_{ec}}\right)^{\gamma-1}\right) \quad (8)$$

In Eqs. (3–8), R and θ are polar coordinates with the origin at the center of the thruster exit plane, $\theta_{1/2}$ is the thruster beam divergence, γ is the plasma polytropic index that we set to 1.3, and subscript c refers to the centerline or reference value. We assume that the model form of the plasma potential is always true, no matter the bias voltage of the axial plate, and thus the plasma potential in the chamber has a fixed spatial distribution. This can be considered true to the first order because the expanding plume structure described by the model is set up by the operation of the thruster, and the measured plasma potential profile (Fig. 12) has approximately the same plasma potential spatial distribution relative to other positions.

The chamber wall and axial plate are paneled as a series of rings of 0.1 m width. At each boundary panel, the ion flux, electron density, electron temperature, and plasma potential are calculated from Eqs. (3–8). We then calculate the ion current to the panel from the ion flux assuming singly charged ions [Eq. (9)] and the electron current to the panel [Eq. (10)]:

$$I_i = j_i e A \quad (9)$$

$$I_e = \begin{cases} \frac{1}{4} n_e e A \sqrt{\frac{8k_B T_e}{\pi m_e}} \exp\left(\frac{e(\phi_w - \phi)}{k_B T_e}\right) & \phi_w < \phi \\ \frac{1}{4} n_e e A \sqrt{\frac{8k_B T_e}{\pi m_e}} & \phi_w \geq \phi \end{cases} \quad (10)$$

We then solve numerically for the value of plasma potential that equalizes the total ion and electron currents lost from the plasma to all panels. Figure 14 shows the result for the plasma potential 1 m from the thruster compared to the experimental data. Figure 15 shows the collected current on the axial plate compared to the experimental data.

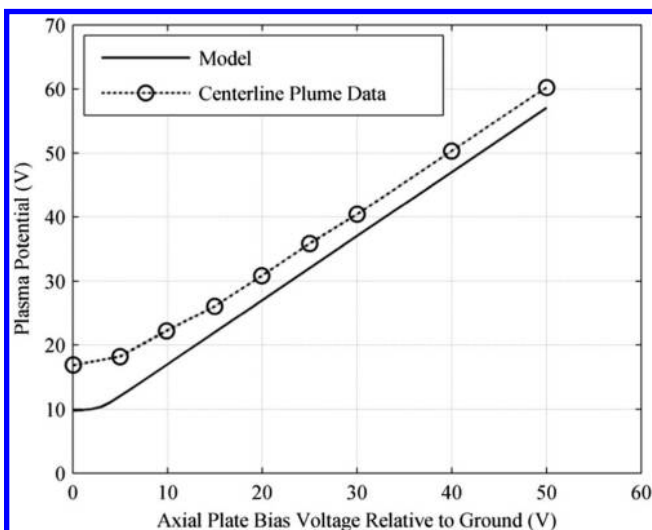


Fig. 14 Plasma potential as a function of axial plate bias voltage: model versus experiment.

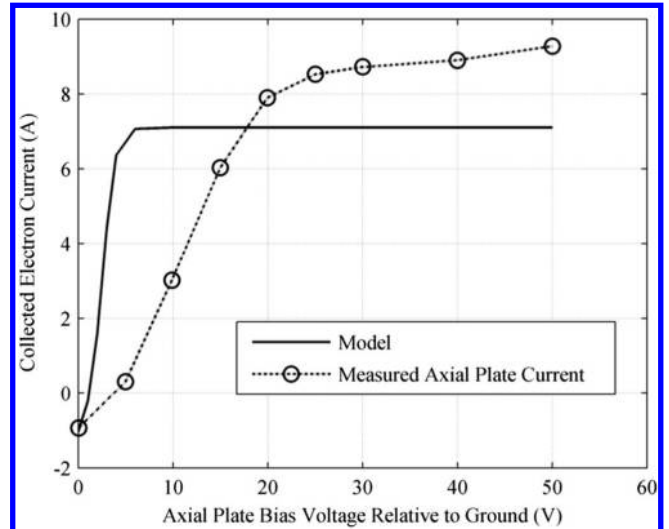


Fig. 15 Axial plate current collected as a function of applied bias voltage: model versus experiment.

Figure 14 shows that the plasma potential behavior in the model agrees well with experimental data and shows a 3–4 V offset between the model and the experimental data. The remaining offset between the model and the experiment may result from collisional effects changing the plasma scaling in the far-field region, where the charge–exchange background plasma becomes significant with respect to the expanding-plume plasma. It may also be due to the simplified assumed geometry, which neglects ion and electron fluxes to detailed chamber features such as the central I beam and personnel support grating. Figure 15 shows that the collected current agrees qualitatively, but all of the cathode electrons are theoretically collected at a much lower bias voltage than is observed experimentally. This is most likely because the model does not take into account collisional effects and the charge–exchange background plasma. In the model, the plasma density is very low at chamber wall surfaces that are not directly impinged by the beam where, in reality, the plasma is denser at the walls due to charge–exchange collisions and the associated diffusion of the plasma. This in turn means that the plate does not collect all the electrons until a higher bias voltage.

It is important to note that secondary electron emission effects on the aluminum chamber plate collected current are neglected in the model for the following reasons: Electron energy distribution measurements of the secondary electron emission (SEE) of aluminum (from Baglin et al. [39], Pillon et al. [40], and Yamauchi and Shimizu [41]) show that the energy distribution of secondary electrons is to the first-order invariant of incoming energy of electrons or ions, and the maximum energy of these electrons is on the order of 15 eV with a most probable energy on the order of 3–4 eV. This means that electrons produced via SEE from the aluminum plate do not have enough energy to overcome the potential difference between the biased axial chamber plate and the surrounding plasma, and they are recollected by the axial chamber plate. The overall first-order net effect is that electrons produced by the SEE from the aluminum chamber plate do not influence the current collection measured. The collected current in the model does not increase above the cathode electron current because additional electrons gained from other chamber sources are not included in the model. At the axial chamber plate biases greater than 20 V, there is an experimentally measured current collection that is well outside what is known to be generated by the HCT beam; therefore, it is concluded that an electrical circuit is formed between the axial chamber plate and the grounded vacuum chamber surfaces through the plasma.

B. Electrical Facility Interaction

The bias voltage of the axial chamber plate is able to control the electron termination pathways of the HCT plume. When the axial plate is grounded, electrons sourced from the cathode are driven

electrostatically into the plume and are collected onto grounded chamber surfaces. This includes the electron current collected onto a grounded thruster body. As the axial chamber plate electron current collection surpasses the available beam current of the HCT, the cathode potential (relative to ground) floats above ground due to the increase in the global plasma potential, as shown in Figs. 10, 12, and 14. Due to the adverse potential gradient between the grounded chamber walls and the cathode-to-ground voltage, electron termination on grounded chamber surfaces diminishes. Figure 16 shows that the decrease in collected electron current on grounded surfaces is also seen in the collected electron current on the grounded thruster body. The floating potential of the electrically floating thruster body also begins to shift positive to attract additional electron flux to maintain a zero net current condition.

At axial plate bias voltages above 20 V, 100% of the HCT beam current is collected on the axial chamber plate, but electron current collection continues to increase with increases in axial chamber plate bias voltage. As demonstrated by the first-order analysis of the current collection on the axial plate (shown in Fig. 15), grounded chamber surfaces are possible sources for these electrons due to field emission or secondary electron emission from chamber surfaces to the plume plasma, because increasing the axial chamber plate bias voltage increases the potential gradient between the plasma and the grounded chamber. As the potential gradient between the chamber wall and the plasma increases, at bias voltages above 40 V, arcing events are witnessed on grounded chamber surfaces. These arcing events indicate a momentary discharge between grounded surfaces

and the ambient plasma. At axial plate bias voltages greater than 40 V, the potential gradient between the plasma potential and grounded chamber surfaces drives all electrons away from grounded surfaces. This potential difference removes the vacuum chamber as an effective electron termination pathway and allows grounded chamber surfaces to become a source of electrons. Figure 17 is a graphical representation of the electron termination pathways for the aforementioned three axial chamber plate bias voltages.

C. Impact of the Axial Chamber Plate Electrical Power

As seen from radial chamber plate current measurements (Fig. 8) and plasma potential measurements near the radial plate (Fig. 9), electrons are driven away from grounded surfaces due to the increased potential difference between the facility walls. The decrease in electron current to grounded surfaces is more indicative of a spacelike environment [18,42]. According to Korsun et al. [18], testing in a ground-facility environment produces a secondary plasma that interacts with the facility walls, and currents “leak” out of the HCT plume into this secondary plasma. These currents represent a loss of energy from the HCT plume into the vacuum chamber walls. With the axial chamber plate, the forced collection of electrons provides additional energy into the plume. By multiplying the current and the voltage of the axial chamber plate, the power being introduced by the axial chamber plate is calculated and shown in Fig. 18. Based on the data presented in this investigation, it is within

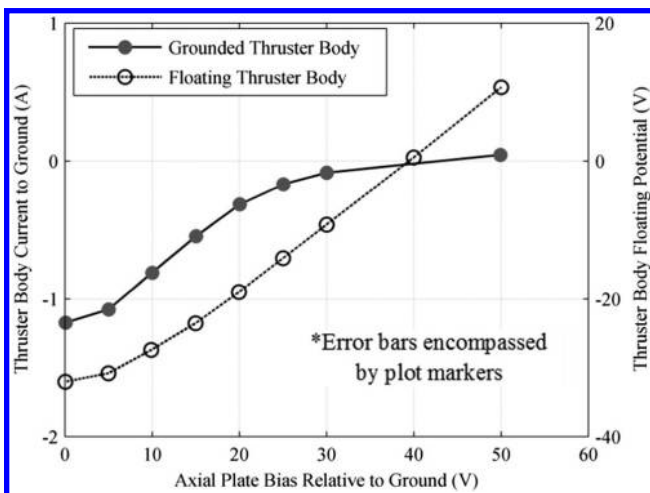


Fig. 16 Thruster body current to ground and thruster body floating voltage as a function of axial plate bias.

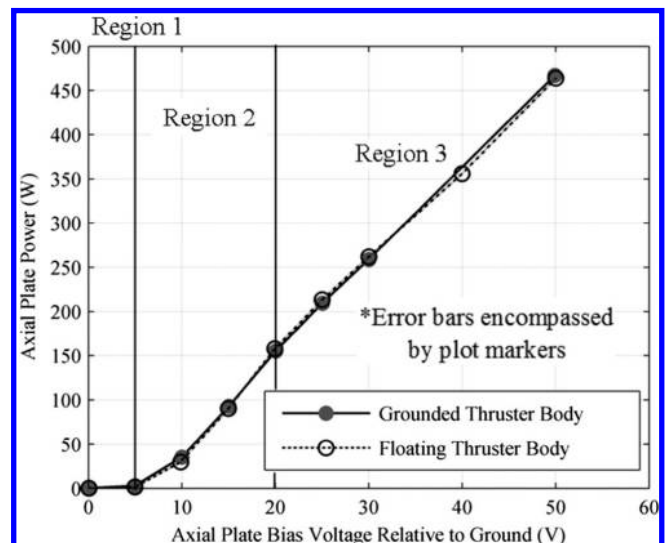


Fig. 18 Power sourced by the axial chamber plate for both thruster electrical configurations.

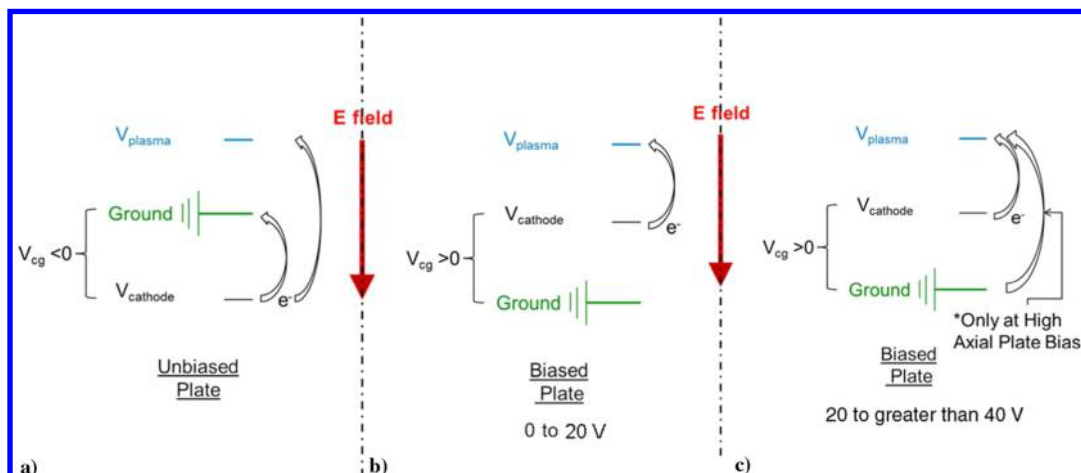


Fig. 17 Notional diagram of electron pathways: a) no axial plate bias voltage or nominal condition, b) low axial plate bias voltage, and c) high axial plate bias voltage.

reason to conclude that the power introduced by the axial chamber plate, in manipulation of the electron termination pathways, helps offset the energy normally lost to conductive grounded surfaces. The compensation of power loss to the conductive walls of the vacuum chamber helps make the HCT plume more representative of the onorbit environment.

D. Enhanced Current Density in the Offaxis Plume

As shown in Fig. 11, the offaxis region of the plume has a current density that is influenced by the axial chamber plate bias voltage. As stated earlier, the Faraday probe has a fixed electron repulsion voltage throughout the testing; therefore, it is not immediately clear if the measured increase in the current density profile is due to changes in the plume or as a result of the Faraday probe fixed electron repulsion voltage. Without further modeling, the increase in current collected on the Faraday probe due to the increase in the potential gradient between the probe and the plasma cannot be estimated. In Fig. 19, data are presented that offer an alternative means of assessing the validity of the measured current density in the offaxis region of the plume. Faraday probe sweeps are taken at four different cathode radial locations relative to thruster centerline: 18.1 (nominal position), 21.9, 27.0, and 43.4 cm. At the cathode nominal position and an axial chamber plate bias of 50 V, the current density is

approximately 25% higher as compared to values measured for the grounded axial chamber plate condition. At other cathode positions, the increase in current density is on the order of 45–50% relative to current densities measured for the grounded axial chamber plate conditions. This variation of behavior in the current density measured is enough to suggest that the increase in current density measured for high axial chamber plate voltages is due in part to actual changes in the HCT plume.

E. Comparison to the Small Missions for Advanced Research in Technology-1 Mission

From the perspective of the HCT electrical circuit, the bias voltage of the axial chamber plate acts to enforce a pseudo-far-field plasma potential boundary condition. The axial plate is able to drive the plasma potential by mediating the electron-ion loss rate to the facility walls. The resulting increase in plasma potential and cathode-to-ground potential is similar to behavior observed during the SMART-1 mission [12,13]. The plasma potential, during the SMART-1 mission, was measured using the electric propulsion diagnostic package (EPDP) and placed downstream from the thruster exit plane and in a “low” ion-energy region of the PPS-1350 plume [43]. The measured difference between the cathode-to-ground voltage and the plasma potential remained approximately 19 V [13] throughout the mission.

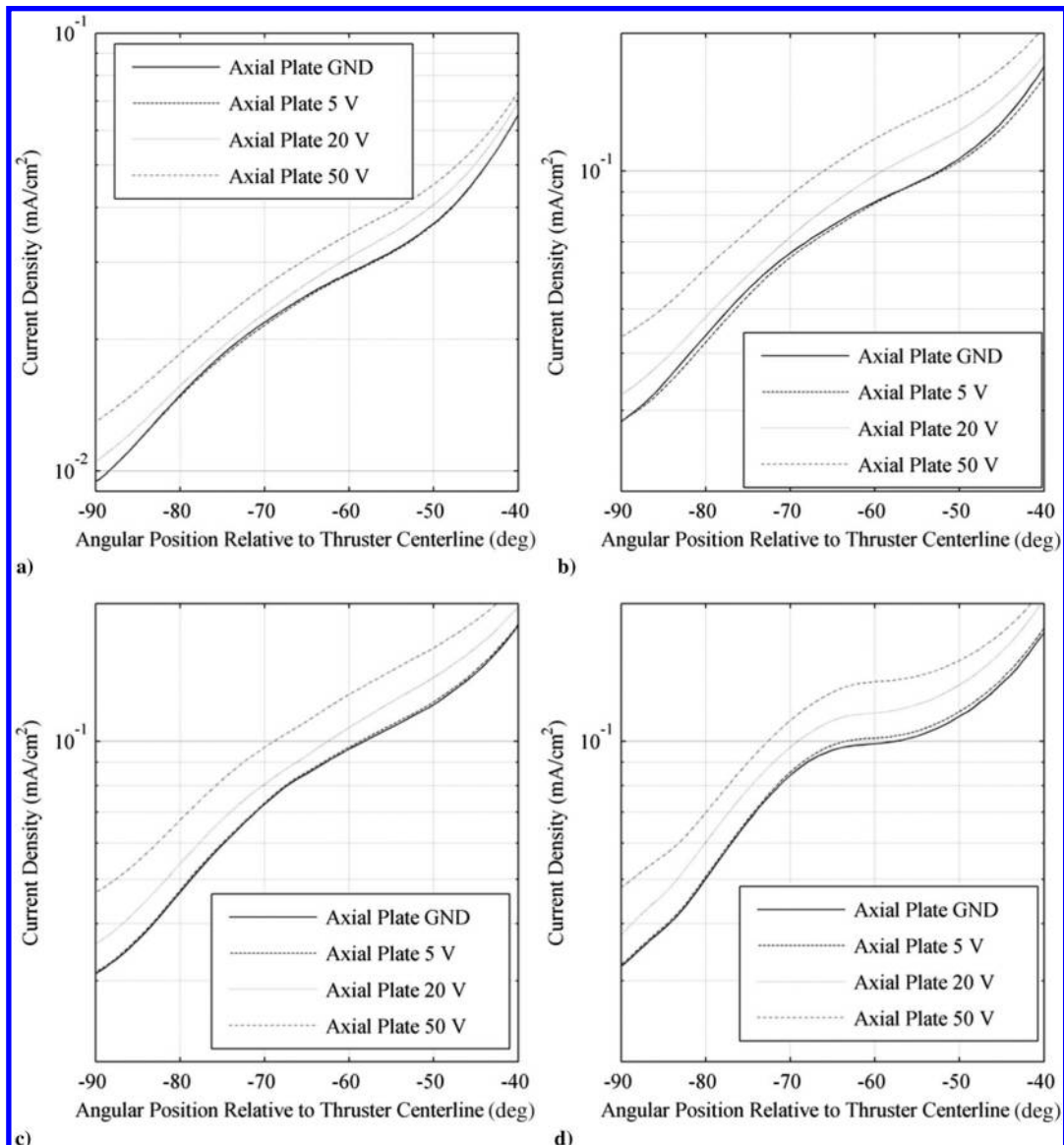


Fig. 19 Current density profiles in the offaxis region of the HCT plume for varying cathode positions relative to thruster centerline: a) 18.1 cm, b) 21.9 cm, c) 27.0 cm, and d) 43.4 cm.

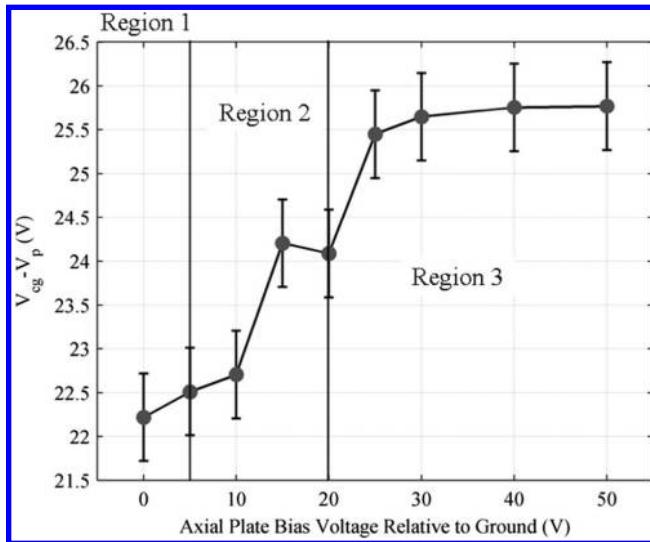


Fig. 20 Potential difference between plasma potential and cathode-to-ground potential as a function of axial plate bias voltage.

As shown in Fig. 10, there is a similar fixed voltage difference between the HCT floating voltage and the centerline plasma potential. The influence on the axial chamber plate on the HCT floating circuit voltage and plasma potential is only evident once the axial chamber plate is able to collect a net electron current. Due to the high mobility of the electrons versus xenon ions, this occurs at a low (greater than 5 V) voltage above ground. Once the axial plate bias voltage is able to establish net electron current collection, the axial chamber plate begins to induce global changes in the HCT plume and HCT electrical circuit. Overall, the potential difference behavior between the plasma potential and the cathode-to-ground potential for the T-140 HCT tested is similar to the behavior experienced by the PPS-1350 in-flight operation.

A closer examination of the data collected in this experiment reveals that the difference between the plasma potential and the cathode-to-ground voltage has a small dependence on the axial chamber plate bias. The difference between the plasma potential at an angular position of -45° relative to thruster centerline and cathode-to-ground potential is shown in Fig. 20. Given the placement of the EPDP, this angular position is in a similar region of the HCT beam. At lower axial chamber plate biases (0–15 V), where the beam current is not fully collected by the plate, there is an increase in this voltage difference by approximately 1–2 V as compared to the nominal case. At higher axial chamber plate biases (20–50 V), the difference between the cathode-to-ground voltage and the plasma potential increases by approximately 2–4 V relative to the nominal condition. This voltage difference behavior is consistent with trends observed at other angular positions. The increase in the potential difference will result in a change in thrust of the T-140 that will be smaller than the resolution of the calibration of the thrust stand used in this investigation and is consistent with expectations based on the work of Frieman et al. [20]. Though the change in thrust is not measurable with the thrust stand used in this investigation, the change in the potential difference between the cathode and the ambient plasma potential is indicative of a change in the efficiency of the HCT electrical circuit in extracting electrons from the cathode [29]. In connection to the in-flight environment, the HCT plasma potential is heavily influenced by the interaction with any charged surfaces, such as the unshielded low-voltage solar panel contacts as seen in the SMART-1 mission [12,13]. As seen in this investigation, a variation in the plasma potential boundary condition relative to the HCT will result in changes to cathode coupling efficiency.

V. Conclusions

This investigation reveals the impact of biasing a downstream electrode on a Hall current thruster (HCT) in a vacuum chamber environment. The bias of a downstream electrode is able to induce

global changes to the HCT plume and impacts the electron termination pathways. At an axial chamber plate electron current collection below the HCT beam current, the resultant change in HCT behavior is consistent with observed in-flight behavior. The axial chamber plate is able to drive global changes in the plasma potential that affect the floating voltage of the HCT circuit and the available electron termination pathways. As shown through first-order analysis, there is electron current collected on the axial chamber plate that is not sourced from the HCT, but it is relatively small compared to the incident beam current. At an axial chamber plate electron current collection well beyond above the HCT beam current, grounded chamber surfaces become a source for electrons due to the electrostatic potential gradient between the grounded facility walls and the local plasma potential. Such a source of electrons is not representative of the space environment and augments the electrostatic acceleration potential by a few volts. The overall results of this work show that, by biasing an electrode in the downstream plume of the HCT above the chamber ground, the net electron current collection on the grounded chamber surfaces and thruster surfaces can be eliminated and global changes in the plasma potential can have an effect on cathode coupling efficiencies.

Acknowledgments

Jonathan Walker is supported by National Science Foundation Graduate Research Fellowships under grant no. DGE-1148903. The authors would like to thank Natalie Schloeder and Aaron Schinder for their assistance in the collection of data for and in preparation of this paper. Jonathan Walker, Samuel Langendorf, and Mitchell Walker would like to acknowledge the Lockheed Martin Space Systems Company for support of this investigation.

References

- [1] Walker, M. L. R., and Gallimore, A. D., "Neutral Density Map of Hall Thruster Plume Expansion in a Vacuum Chamber," *Review of Scientific Instruments*, Vol. 76, No. 5, 2005, Paper 053509. doi:10.1063/1.1915011
- [2] Kamhawi, H., Huang, W., Haag, T., and Spektor, R., "Investigation of the Effects of Facility Background Pressure on the Performance and Operation of the High Voltage Hall Accelerator," *50th AIAA/ASME/SAE/ASEE Joint Propulsion Conference*, AIAA Paper 2014-3707, July 2014.
- [3] Huang, W., Kamhawi, H., Lobbia, R. B., and Brown, D. L., "Effect of Background Pressure on the Plasma Oscillation Characteristics of the HiVHAc Hall Thruster," *50th AIAA/ASME/SAE/ASEE Joint Propulsion Conference*, AIAA Paper 2014-3708, July 2014.
- [4] Diamant, K., Spektor, R., Beiting, E., Young, J., and Curtiss, T., "The Effects of Background Pressure on Hall Thruster Operation," *48th AIAA/ASME/SAE/ASEE Joint Propulsion Conference and Exhibit*, AIAA Paper 2012-3735, July 2012.
- [5] Hofer, R. R., and Anderson, J. R., "Finite Pressure Effects in Magnetically Shielded Hall Thrusters," *50th AIAA/ASME/SAE/ASEE Joint Propulsion Conference*, AIAA Paper 2014-3709, 2014.
- [6] Diamant, K. D., Liang, R., and Corey, R. L., "The Effect of Background Pressure on SPT-100 Hall Thruster Performance," *50th AIAA/ASME/SAE/ASEE Joint Propulsion Conference*, AIAA Paper 2014-3710, 2014.
- [7] Nakles, M. R., and Hargus, W. A., Jr., "Background Pressure Effects on Ion Velocity Distribution Within a Medium-Power Hall Thruster," *Journal of Propulsion and Power*, Vol. 27, No. 4, 2011, pp. 737–743. doi:10.2514/1.48027
- [8] Brown, D. L., and Gallimore, A. D., "Evaluation of Facility Effects on Ion Migration in a Hall Thruster Plume," *Journal of Propulsion and Power*, Vol. 27, No. 3, 2011, pp. 573–585. doi:10.2514/1.B34068
- [9] Walker, M. L. R., Victor, A. L., Hofer, R. R., and Gallimore, A. D., "Effect of Backpressure on Ion Current Density Measurements in Hall Thruster Plumes," *Journal of Propulsion and Power*, Vol. 21, No. 3, 2005, pp. 408–415. doi:10.2514/1.7713
- [10] Walker, M. L. R., "Effects of Facility Backpressure on the Performance and Plume of a Hall Thruster," Ph.D. Dissertation, Aerospace Engineering, Univ. of Michigan, Ann Arbor, MI, 2005.
- [11] Hofer, R. R., Peterson, P. Y., and Gallimore, A., "Characterizing Vacuum Facility Backpressure Effects on the Performance of a Hall

- Thruster," *27th International Electric Propulsion Conference*, Electric Rocket Propulsion Soc. IEPC Paper 01-045, Fairview Park, OH, 2001.
- [12] Passaro, A., Vicini, A., Nania, F., and Biagioni, L., "Numerical Rebuilding of SMART-1 Hall Effect Thruster Plasma Plume," *Journal of Propulsion and Power*, Vol. 26, No. 1, 2010, pp. 149–158. doi:10.2514/1.36821
- [13] Koppel, C., Marchandise, F., Estublier, D., and Jolivet, L., "The Smart-1 Electric Propulsion Subsystem In Flight Experience," *40th AIAA/ASME/SAE/ASEE Joint Propulsion Conference and Exhibit*, AIAA Paper 2004-3435, 2004.
- [14] Boyd, I. D., and Dressler, R. A., "Far Field Modeling of the Plasma Plume of a Hall Thruster," *Journal of Applied Physics*, Vol. 92, No. 4, 2002, pp. 1764–1774. doi:10.1063/1.1492014
- [15] Manzella, D. H., Jankovsky, R., Elliot, F., Mikellides, I., Jongeward, G., and Allen, D., "Hall Thruster Plume Measurements On-board the Russian Express Satellites," *27th International Electric Propulsion Conference*, Electric Rocket Propulsion Soc. IEPC Paper 2001-044, Fairview Park, OH, 2001.
- [16] Walker, J. A., Frieman, J. D., Walker, M. L. R., Khayms, V., King, D., and Peterson, P. Y., "Electrical Facility Effects on Hall-Effect-Thruster Cathode Coupling: Discharge Oscillations and Facility Coupling," *Journal of Propulsion and Power*, Vol. 32, No. 4, 2016, pp. 844–855. doi:10.2514/1.B35835
- [17] Frieman, J. D., Walker, J. A., Walker, M. L. R., Khayms, V., and King, D., "Electrical Facility Effects on Hall Effect Thruster Cathode Coupling: Performance and Plume Properties," *Journal of Propulsion and Power*, Vol. 32, No. 1, 2016, pp. 251–264. doi:10.2514/1.B35683
- [18] Korsun, A. G., Tverdokhlebova, E. M., and Gabdullin, F. F., "The Distinction Between the EP Plume Expansion in Space and in Vacuum Chamber," *29th International Electric Propulsion Conference*, Electric Rocket Propulsion Soc. IEPC Paper 2005-073, Fairview Park, OH, 2005.
- [19] Tremolizzo, E., Meier, H., and Estublier, D., "In-Flight Disturbance Torque Evaluation of the Smart-1 Plasma Thruster," *Proceedings of the 18th International Symposium on Space Flight Dynamics*, Vol. 548, 2004, pp. 303–306.
- [20] Frieman, J. D., King, S. T., Walker, M. L. R., Khayms, V., and King, D., "Role of a Conducting Vacuum Chamber in the Hall Effect Thruster Electrical Circuit," *Journal of Propulsion and Power*, Vol. 30, No. 6, 2014, pp. 1471–1479. doi:10.2514/1.B35308
- [21] Walker, J. A., Frieman, J. D., Walker, M. L., Khayms, V., King, D., and Peterson, P., "Electrical Facility Effects on Hall Effect Thruster Cathode Coupling: Discharge Oscillations and Facility Coupling," *50th AIAA/ASME/SAE/ASEE Joint Propulsion Conference*, AIAA Paper 2014-3711, 2014.
- [22] Kieckhafer, A., and Walker, M. L. R., "Recirculating Liquid Nitrogen System for Operation of Cryogenic Pumps," *32nd International Electric Propulsion Conference*, IEPC Paper 2011-217, 2011.
- [23] Tilford, C. R., "Sensitivity of Hot Cathode Ionization Gages," *Journal of Vacuum Science and Technology, A*, Vol. 3, No. 3, 1985, pp. 546–550. doi:10.1116/1.572991
- [24] "571 Ionization Gauge Tube Instruction Manual," Manual No. 699990571, Rev. C, Agilent Technologies Vacuum Products Division, Lexington, MA, 2002.
- [25] McLean, C., McVey, J., and Schappell, T., "Testing of a U.S.-Built HET System for Orbit Transfer Applications," *35th Joint Propulsion Conference and Exhibit*, AIAA Paper 1999-2574, 1999.
- [26] Snyder, J. S., Baldwin, J., Frieman, J. D., Walker, M. L. R., Hicks, N. S., Polzin, K. A., and Singleton, J. T., "Flow Control and Measurement in Electric Propulsion Systems: Towards an AIAA Reference Standard," *33rd International Electric Propulsion Conference*, Electric Rocket Propulsion Soc. IEPC Paper 2013-425, Fairview Park, OH, 2013.
- [27] Spektor, R., Willhoff, M. A., Beiting, E., and Diamant, K., "Characterization of the High Power Propulsion System Subscale," *60th JANNAF Propulsion Meeting*, Johns Hopkins Univ. JANNAF Paper 2013-3142, Baltimore, MD, 2013.
- [28] Xu, K. G., and Walker, M. L. R., "High-Power, Null-Type, Inverted Pendulum Thrust Stand," *Review of Scientific Instruments*, Vol. 80, No. 5, 2009, Paper 055103. doi:10.1063/1.3125626
- [29] Goebel, D. M., and Katz, I., *Fundamentals of Electric Propulsion: Ion and Hall Thrusters*, Wiley, Hoboken, NJ, 2008, pp. 24, 124–133, 342, 408–411.
- [30] Sheehan, J. P., and Hershkovitz, N., "Emissive Probes," *Plasma Sources Science and Technology*, Vol. 20, No. 6, 2011, pp. 1–22. doi:10.1088/0963-0252/20/6/063001
- [31] Demidov, V. I., Ratynskaia, S. V., and Rypdal, K., "Electric Probes for Plasmas: The Link Between Theory and Instrument," *Review of Scientific Instruments*, Vol. 73, No. 10, 2002, pp. 3409–3439. doi:10.1063/1.1505099
- [32] Hutchinson, I. H., *Principles of Plasma Diagnostics*, Cambridge Univ. Press, New York, 2002.
- [33] Hofer, R. R., Walker, M. L. R., and Gallimore, A., "A Comparison of Nude and Collimated Faraday Probes for Use with Hall Thrusters," *27th International Electric Propulsion Conference*, Electric Rocket Propulsion Soc. IEPC Paper 2001-020, Fairview Park, OH, 2001.
- [34] Brown, D. L., "Investigation of Low Discharge Voltage Hall Thruster Characteristics and Evaluation of Loss Mechanisms," Ph.D. Dissertation, Aerospace Engineering, Univ. of Michigan, Ann Arbor, MI, 2009.
- [35] Brown, D. L., and Gallimore, A. D., "Evaluation of Ion Collection Area in Faraday Probes," *Review of Scientific Instruments*, Vol. 81, No. 6, 2010, Paper 063504. doi:10.1063/1.3449541
- [36] Ekholm, J., and Hargus, W., " $E \times B$ Measurements of a 200 W Xenon Hall Thruster," *41st AIAA/ASME/SAE/ASEE Joint Propulsion Conference and Exhibit*, AIAA Paper 2005-4405, 2005.
- [37] Korsun, A., and Tverdokhlebova, E., "The Characteristics of the EP Exhaust Plume in Space," *33rd Joint Propulsion Conference and Exhibit*, AIAA Paper 1997-3065, 1997.
- [38] Azziz, Y., "Instrument Development and Plasma Measurements on a 200-Watt Hall Thruster Plume," M.S. Thesis, Aeronautics and Astronautics, Massachusetts Inst. of Technology, Cambridge, MA, 2001.
- [39] Baglin, V., Bojko, J., Grobner, O., Henrist, B., Hilleret, N., Scheurlein, C., and Taborelli, M., "The Secondary Electron Yield of Technical Materials and its Variation with Surface Treatments," *7th European Particle Accelerator Conference*, Large Hadron Collider Project Rept. 433, European Organization for Nuclear Research, Vienna, 2000.
- [40] Pillon, J., Roptin, D., and Cailler, M., "Secondary Electron Emission from Aluminium," *Surface Science*, Vol. 57, No. 2, 1976, pp. 741–748. doi:10.1016/0039-6028(76)90359-9
- [41] Yamauchi, Y., and Shimizu, R., "Secondary Electron Emission from Aluminum by Argon and Oxygen Ion Bombardment Below 3 keV," *Japanese Journal of Applied Physics*, Vol. 22, No. 4A, 1983, Paper L227.
- [42] Anatoly, K., Ekaterina, T., Flur, G., and Sylvia, B., "The Electric Currents and Potentials Generated by Plasma Plume over SC Structure Elements," *42nd AIAA Aerospace Sciences Meeting and Exhibit*, AIAA Paper 2004-0985, 2004.
- [43] Matticari, G., Noci, G., Estublier, D., del Amo, J. G., Marini, A., and Tajmar, M., "The SMART-1 Electric Propulsion Diagnostic Package," *Third International Conference on Spacecraft Propulsion*, Vol. 465, Aeronautique Astronautique de France, Paris, France, 2000, pp. 661–668.

J. Blandino
Associate Editor